Shear Ordering in Thin Films of Spherical Block Copolymer

Gaurav Arya,*,† Jörg Rottler,‡ Athanassios Z. Panagiotopoulos,†,‡ David J. Srolovitz,‡,§ and Paul M. Chaikin‡,||,⊥

Department of Chemical Engineering, Princeton Institute for the Science and Technology of Materials, Department of Mechanical and Aerospace Engineering, and Department of Physics, Princeton University, Princeton, New Jersey 08544, U.S.A.

Received June 19, 2005. In Final Form: September 16, 2005

We have investigated shear-induced alignment of a bilayer of spherical diblock copolymer micelles within thin films using molecular dynamics simulations at two different levels of coarse-graining. At the microscopic level, the copolymers are modeled as bead and spring chains with specific interaction potentials which produce strongly segregated spherical micelles. The simulations qualitatively reveal that long-range shear-induced ordering of hexagonally arranged micelles arises because of the tendency of micelles to pursue trajectories of minimum frictional resistance against micelles in the opposing layer. This influences their alignment in the direction of shear without them breaking apart and reforming within the time scale of the simulations. As observed in experiments, the ordering is shown to be very sensitive to the film thickness and shearing rates. To access larger lengths and longer time scales, we further coarse-grain our system to a mesoscopic level where an individual micelle is represented by a spherical particle, which interacts with other micelles through an effective potential obtained from the microscopic simulations. This approach enables us to follow the time evolution of global order from locally ordered domains. An exponentially fast growth of the orientational correlation length of the hexagonal pattern at early times, followed by a crossover to linear growth, is found in the presence of shear, in contrast to the much slower power-law scalings observed in experiments without shear.

1. Introduction

Block copolymers comprise two or more chemically distinct and mutually immiscible polymer chains (blocks) that are covalently bonded together. They readily self-assemble into repeating nanometer-sized spherical, cylindrical, gyroid-like, or lamellar microphases at temperatures below their order−disorder transition temperature T_{odt} and above their glass transition temperature T_g.[1] Because of their regular nanostructured nature, block copolymer thin films have been recognized as ideal templates for synthesizing a range of nanostructures including quantum dots, metal nanowires, and photonic waveguides.[2,3]

Unfortunately, the coarsening of block copolymer microphases into well-ordered lattices tends to be very slow under regular annealing conditions (especially in the defect-annihilation regime), and hence, long-range orientational order is rarely achieved in practice.[4−6] Several methods have been proposed to accelerate the kinetics of alignment and promote long-range order, including the application of shear[7] or electric fields[8] and the use of chemically patterned substrates.[9] The most promising and simplest of these approaches involves the use of steady or oscillatory shear. This method has shown considerable success in aligning spherical,[10,11] cylindrical,[12,13] and lamellar[14−16] block copolymer microphases in the bulk. It is only very recently that steady shear has been employed to improve the degree of alignment of cylindrical[17] and spherical microphases[18] in thin films. In the former study, a monolayer of cylindrical microphases on a silicon substrate aligned in the direction of shear over areas as large as 1 cm × 1 cm. In the second study, a thin film containing exactly two layers (bilayer) of hexagonally ordered (triangular lattice) spherical block copolymer microphases was shown to align in response to shear, where one of the basis vectors of the lattice orients in the shear direction.

* Corresponding author. E-mail: garya@nyu.edu. Current address: Department of Chemistry, New York University, 31 Washington Place Rm. 1001, New York, NY 10003, USA.
† Department of Chemical Engineering.
‡ Princeton Institute for the Science and Technology of Materials.
§ Department of Mechanical and Aerospace Engineering.
|| Department of Physics.
⊥ Current address: Department of Physics, New York University, 4 Washington Place, New York, NY 10003, USA.

(1) Matsen, M. W.; Bates, F. S. *Macromolecules* **1996**, *29*, 1091.
(2) Park, M.; Harrison, C.; Chaikin, P. M.; Register, R. A.; Adamson, D. H. *Science* **1997**, *276*, 1401.
(3) Cheng, J. Y.; Mayes, A. M.; Ross, C. A. *Nat. Mater.* **2004**, *3*, 823.
(4) Newstein, M. C.; Garetz, B. A.; Balsara, N. P.; Chang, M. Y.; Dai, H. J. *Macromolecules* **1998**, *31*, 64.
(5) Harrison, C.; Cheng, Z.; Sethuraman, S.; Huse, D. A.; Chaikin, P. M.; Vega, D. A.; Sebastian, J. M.; Register, R. A.; Adamson, D. H. *Phys. Rev. E* **2002**, *66*, 011706.
(6) Arya, G.; Panagiotopoulos, A. Z. *Phys. Rev. E* **2004**, *70*, 031501.
(7) Hamley, I. W. *J. Phys.: Condens. Matter* **2001**, *13*, R643.
(8) Morkved, T. L.; Lu, M.; Urbas, A. M.; Ehrichs, E. E.; Jaeger, H. M.; Mansky, P.; Russell, T. P. *Science* **1996**, *273*, 931.
(9) Kim, S. O.; Solak, H. H.; Stoykovich, M. P.; Ferrier, N. J.; de Pablo, J. J.; Nealey, P. F. *Nature (London)* **2003**, *424*, 411.
(10) Almdal, K.; Koppi, K.; Bates, F. S. *Macromolecules* **1993**, *26*, 4058.
(11) McConnell, G. A.; Lin, M. Y.; Gast, A. P. *Macromolecules* **1995**, *28*, 6754.
(12) Hadziioannou, G.; Mathis, A.; Skoulios, A. *Colloid Polym. Sci.* **1979**, *257*, 136.
(13) Scott, D. B.; Waddon, A. J.; Lin, Y.; Karasz, F. E.; Winter, H. H. *Macromolecules* **1992**, *25*, 4175.
(14) Koppi, K.; Tirrel, M.; Bates, F. S. *Phys. Rev. Lett.* **1993**, *70*, 1449.
(15) Winey, K. I.; Patel, S. S.; Larson, R. G.; Watanabe, H. *Macromolecules* **1993**, *26*, 2542.
(16) Chen, Z.-R.; Issain, A. M.; Kornfield, J. A.; Smith, S. D.; Grothaus, J. T.; Satkowski, M. M. *Macromolecules* **1997**, *30*, 7096.
(17) Angelescu, D. E.; Waller, J. H.; Adamson, D. H.; Deshpande, P.; Chou, S. Y.; Register, R. A.; Chaikin, P. M. *Adv. Mater.* **2004**, *16*, 1736.
(18) Angelescu, D. E.; Waller, J. H.; Register, R. A.; Chaikin, P. M. *Adv. Mater.* **2005**, *16*, 1878.

10.1021/la0516476 CCC: $30.25
Published on Web 10/26/2005

It is generally assumed (though yet to be proven) that the microphases align in the velocity direction in order to minimize the overall shear stress within the system. For instance, it was hypothesized in ref 18 that the spherical microphase pattern adjusts (rotates) itself in a manner such that the microphases in both the layers flow in the "easy-flow" direction. However, a detailed microscopic picture of the alignment process and a confirmation of this hypothesis are still missing. For example, it is not known whether the microphases gradually annihilate their defects while maintaining their intact structure or whether they shear melt and then re-form to produce alignment. In addition, the process by which the shear-aligned domains grow in size, as well as the growth kinetics, is far from fully understood. Further, it is not clear why the alignment observed in these experiments is so sensitive to the thickness of the film. Films 2% thicker or thinner than the ideal bilayer thickness as well as monolayer-thick films were less well ordered.

In the present study, we address several of these issues in shear-induced alignment of spherical microphases using molecular dynamics simulations at two length scales. Our block copolymers are modeled using a coarse-grained bead and spring model with suitable interactions between the beads to promote microphase separation. Instead of simulating dense, dynamically sluggish and computationally intensive block copolymer melts, we have chosen to simulate the computationally easier system of strongly segregated block copolymers in a selective solvent. As previously demonstrated,[19] the volume fraction of the copolymer ϕ in the solution then takes the role of f in determining the microphase morphology, where f denotes the relative size of the "outer" block in a microphase separated melt with respect to the overall degree of polymerization of the copolymer.[20] Previously,[21] we employed the same model of block copolymers to successfully understand the mechanism of alignment in thin films of cylindrical micelles.

Our coarse-grained microscopic simulations are not able to provide a statistically accurate description of the growth of the hexagonally ordered domains because of severe computational limitations of molecular-based models. To overcome this shortcoming, we have adopted a multiscale modeling approach whereby the micelles are further coarse-grained as spherical particles with an interaction potential obtained from the pair distribution function between individual micelles at dilute concentrations. With this approach, we are able to follow the growth of the ordered domains and obtain the relevant correlation lengths and times.

2. Microscopic Model

The diblock copolymers are modeled as linear chains composed of blocks of coarse-grained beads representing corona forming solvophilic headgroups (H) and core-forming solvophobic tail groups (T), based on similar models proposed by other authors.[22−25] It has been shown in refs 22 and 23 that such simple models can effectively model microphase separation of block copolymers in the melt state and in selective solvents. Figure 1 schematically

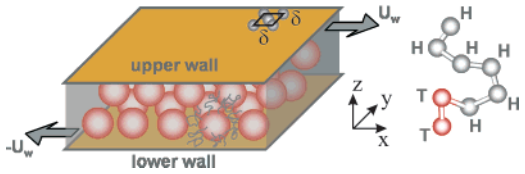

Figure 1. Schematic of the simulation setup showing a bilayer of spherical micelles in solvent confined between two atomistic walls and the off-lattice model adopted for an H_6T_2 surfactant.

shows an H_6T_2 block copolymer chosen for this study, which spontaneously forms fairly stable spherical micelles with the chosen interaction potentials (see below) at the temperatures and densities of interest. The effective diameter of all the beads is denoted by σ. The beads within a polymer chain are connected to each other via a finitely extensible nonlinear elastic (FENE) spring as given by

$$U_{\mathrm{FENE}} = \begin{cases} -\frac{1}{2}kR_0^2 \ln[1-(r/R_0)^2] & r < R_0 \\ \infty & r \geq R_0 \end{cases} \quad (1)$$

where r is the distance between the beads, and k and R_0 are the spring constant and its maximum extension, respectively. We set $k = 30\epsilon/\sigma^2$ and $R_0 = 1.5\sigma$, where ϵ is a parameter that sets the energy scale. Each pair of beads, except the T−T pairs, interact with each other through a Weeks−Chandler−Anderson (WCA) short-range purely repulsive potential given by

$$U_{\mathrm{rep}} = \begin{cases} 4\epsilon[(\sigma/r)^{12} - (\sigma/r)^6 + 1/4] & r < 2^{1/6}\sigma \\ 0 & r \geq 2^{1/6}\sigma \end{cases} \quad (2)$$

The T−T bead pairs, on the other hand, interact with each other through a relatively longer ranged potential which has both repulsive and attractive portions

$$U_{\mathrm{att}} = \begin{cases} 4\epsilon[(\sigma/r)^{12} - (\sigma/r)^6 + 1/4] - \Phi & r < 2^{1/6}\sigma \\ \frac{1}{2}\Phi[\cos(\alpha r^2 + \beta) - 1] & 2^{1/6}\sigma \leq r < 1.5\sigma \\ 0 & r \geq 1/5\sigma \end{cases} \quad (3)$$

where the constants $\alpha = 3.173\ 07$ and $\beta = -0.856\ 23$ were chosen to keep the potential continuous and differentiable. The parameter Φ represents the attractive well depth of this potential, which promotes microphase separation of the copolymers, somewhat similar to the Flory−Huggins parameter χ. Note that all quantities in sections 2−4 are expressed in units of σ, ϵ, and m (mass of each bead).[26] A mapping of these time and length scales to real units is discussed in detail later. Also, note that we have chosen to keep the Boltzmann temperature fixed ($k_BT = \epsilon$) and instead modulate the degree of microphase separation using the parameter Φ, which then takes the role of an inverse temperature. For simplicity, the solvent molecules are not included explicitly in the simulations, as their

(19) Lodge, T. P.; Pudil, B.; Hanley, K. J. *Macromolecules* **2002**, *35*, 4707.
(20) For example, consider the H_xT_y block copolymer utilized in this study where the species H form the outer corona of the block copolymer micelles. Adding a solvent which is selective to the corona-forming H blocks, which reduces the polymer volume fraction ϕ, is equivalent to increasing $f = x/(x + y)$.
(21) Arya, G.; Panagiotopoulos, A. Z. *Comput. Phys. Commun.* **2005**, *169*, 262.
(22) Guo, H.; Kremer, K. *J. Chem. Phys.* **2003**, *119*, 9308.
(23) Rychkov, I.; Yoshikawa, K. *Macromol. Theory Simul.* **2004**, *13*, 257.
(24) Milchev, A,; Bhattacharya, A.; Binder, K. *Macromolecules* **2001**, *34*, 1881.
(25) Larson, R. G. *Chem. Eng. Sci.* **1994**, *49*, 2833.
(26) Allen, M. P.; Tildesley, D. J. *Computer Simulation of Liquids*; Clarendon Press: Oxford, 1987.

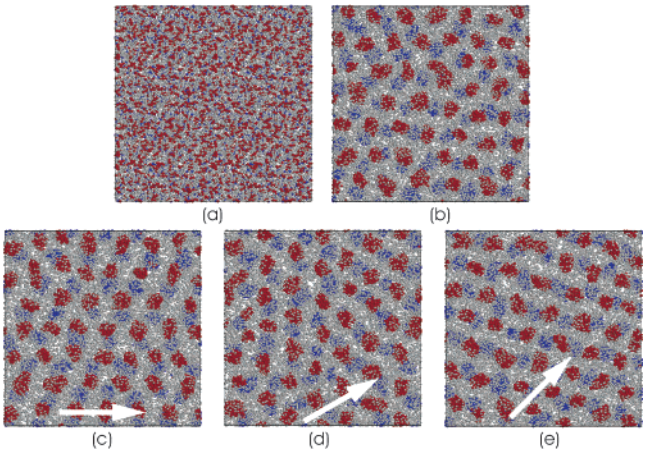

Figure 2. Top view of spherical micelles, composed of an H_6T_2 surfactant, demonstrating shear-induced alignment in the two micelle layers. The head beads are shaded gray, while the tail beads are shaded darker. (a) The disordered starting configuration of surfactants. (b) The final configuration with no imposed shear. (c)−(e) The final micelle configurations after shearing at 0°, 30°, and 45° with respect to the horizontal (shown by the white arrows).

effect (mainly that of shifting microphase transition boundaries) would not add to the phenomena being explored in this study.

The model system is schematically shown on the left-hand side of Figure 1. It consists of a bilayer of spherical diblock copolymer micelles (once formed) confined between two atomistic walls. The two confining walls consist of atoms, identical in their interactions and size to the H beads of the copolymer, arranged as a square lattice with a lattice spacing $\delta = 1.56$ (see Figure 1). The walls are thus repulsive and finely corrugated. The bilayer system is then sheared in the $\pm x$ directions by sliding the walls in opposite directions with identical speeds v_{wall}. Because of collisions between the wall atoms and the enclosed polymer, a Couette-like shear flow is generated. The magnitude of shear stress transmitted to the polymers is controlled by modulating the sliding speed of the walls v_{wall}. Periodic boundary conditions are used in the x and y directions to mimic an infinite system. The simulation box length $L = 60$ was kept much larger than the natural periodicity of the hexagonal pattern formed by the micelles (approximate lattice spacing of $l = 10$; see Figure 2b−e). The polymer density ρ and the temperature were kept fixed in the canonical ensemble simulations. The equations of motion were integrated using a Verlet algorithm with a time step $\delta t = 0.005$. The temperature was maintained constant with the aid of a profile-unbiased Nosé−Hoover thermostat.[27] The simulation box was divided into small cells, and the temperature was calculated in each cell by subtracting the streaming velocity component in that cell.

To ensure that the temperature is being maintained correctly in our simulations, we also calculated the configurational temperature T_{conf}. The configurational temperature was computed using the definitions in ref 28, as given by

$$\frac{1}{k_B T_{conf}} = -\frac{2\langle \sum_{i=1}^{N}\sum_{j>i}^{N} \nabla_{rij}\cdot \mathbf{F}_{ij}\rangle}{\langle \sum_{i=1}^{N} \mathbf{F}_i \cdot \mathbf{F}_i\rangle} \qquad (4)$$

where $\mathbf{F}_i$ is the total force acting on each bead/atom of the system and $\mathbf{F}_{ij}$ is the pairwise force acting between two beads, while N is the total number of beads in the simulation box. At the end of the simulations, the average configurational temperature was compared with the "kinetic" temperature. The configurational and kinetic temperatures were found to always be within 1% of each other at the high shear rate regimes where the thermostats are most prone to systematic errors. Hence, our thermostat efficiently maintains the temperature at the desired set point.

3. Microscopic Shear Ordering Dynamics

The simulations were started from a completely disordered state as shown in Figure 2a. By keeping the polymer density fixed at $\rho = 0.46$ and varying the wall separation h from 13 to 17, the total number of interacting beads in the system (including the beads composing the two confining walls) varied from about 26 000 to 32 500. The segregation strength parameter Φ was maintained at a value of 2.5 throughout, which produces strongly segregated and fairly stable micelles. The simulations were run for a time $t = 5000$ (in reduced units of $\sqrt{m\sigma^2/\epsilon}$), and configurations of the micelles were analyzed at intervals of $\Delta t = 50$. The simulations were therefore computationally intensive, with each simulation run requiring about 6 days of CPU time on an Intel Pentium 4 processor at 1.6 GHz. The typical diameter of the micelles $D = 10.4$ was computed as twice their radius of gyration (including beads composing both the core and the corona of the micelles). Three different shearing directions were used in the simulations, namely, $\theta_0 = 0°, 30°$, and 45°, while the shearing velocities were varied from $v_{wall} = 0.0$ to 5.0.

One may roughly translate the "simulation" units of distances and times to "real" units by associating a length scale to each coarse-grained bead of the copolymer and comparing the self-diffusivity (D_s) of block copolymers computed from simulations with that obtained experimentally, as done previously.[6] Assigning an approximate length scale of 1 nm to the size of each polymer bead (which in our case is roughly equivalent to the Kuhn length of the polymer) and comparing $D_s = 0.02$ computed from our simulations with $D_s \approx 2 \times 10^{-11}$ m^2/s (estimated from experimental diffusivity data on extremely short diblock copolymers[29]), we conclude that 1 time unit in our simulations corresponds to roughly 1 ns. This implies that our coarse-grained simulations are able to roughly sample time scales on the order of microseconds and length scales on the order of 100 nm.

Figure 2b shows the top view of the micelle configuration with $h = 15$ at the end of the simulations at zero shear rate. At the above wall spacing (≃30% smaller than twice the diameter of the micelles), significant overlap between the two oppositely sliding layers of micelles exists. The effect of wall separation on the degree of alignment is discussed in more detail later. The micelles arrange themselves into a hexagonal lattice, albeit with several defects in which some of the micelles are surrounded by 5 or 7 neighboring micelles (dislocations). Other forms of defects related to the intermicellar spacing and bond angles between neighboring micelles are also present in the systems. These defects are more related to the low density of the polymer chosen in this study, and are not topological in nature. Choosing denser systems gave rise to more uniform intermicellar distances and angles, but

(27) Nosé, S. *Prog. Theor. Phys. Suppl.* **1991**, *103*, 1.
(28) Lue, L.; Jepps, O. G.; Delhommelle, J.; Evans, D. J. *Mol. Phys.* **2002**, *100*, 2387.
(29) Yokohama H.; Kramer, E. J. *Macromolecules* **1998**, *31*, 7871.

then yielded extremely sluggish systems which cannot be probed with our computational resources.

Figure 2c−e shows the configuration of micelles at the end of the simulations in which the system was sheared in three different directions with $v_{wall} = 2.0$. Clearly, the micelles seem to have aligned with one of their basis vectors parallel to the shearing direction. One should also note the high degree of registry between the upper and lower layers of micelles. During the simulations, the micelles were observed to make translational adjustments in order to allow micelles in the opposite layer to flow past them (i.e., a form of zigzag motion). This dynamic interaction between the two micelle layers ultimately allows the micelles to align in the "easy-flow" direction, corresponding to an arrangement where both micelle layers form a hexagonal pattern with one of its basis vectors pointing in the shear direction. Within the time scale of the simulation, the micelles did not break up in response to the shear during the alignment process. This is possibly an artifact of the large segregation strengths (Φ) used in our simulations. Nonetheless, the above results demonstrate that the micelles need not break apart (shear-melt) and re-form to yield shear-aligned hexagonally arranged bilayers. Rather, shear alignment may occur by translation of the individual micelles.

The degree of hexagonal ordering within each of the two micelle layers was analyzed using an order parameter Ψ'_6 defined as

$$\Psi'_6 = \frac{6}{\pi}\int_0^{\pi/3}\left(\frac{1}{N_{bonds}}\sum_{i,j}^{N_{bonds}}\cos[6(\theta(\mathbf{r}_{ij}) - \theta')]\right)^2 d\theta' \quad (5)$$

where $\mathbf{r}_{ij} = \mathbf{r}_i - \mathbf{r}_j$ is a vector connecting the center of mass positions of two separate micelles i and j within the same layer, $\theta(\mathbf{r}_{ij})$ is the angle this vector subtends with the x axis, θ' is a variable angle within the range $(0, \pi/3)$, and N_{bonds} is the total number of independent intermicellar vectors present in the two layers. Alternatively, one may quantify ordering on the basis of the standard hexatic order parameter given by

$$\Psi''_6 = \langle\Psi_6(\mathbf{r}_{ij})\rangle = \frac{1}{N_{bonds}}\sum_{i,j}^{N_{bonds}}\exp[6i(\theta(\mathbf{r}_{ij}) - \theta')] \quad (6)$$

where θ' is the angle subtended by a suitable reference axis and the x axis. For sheared systems, this reference axis is naturally the velocity axis; for zero shear simulations, one is deprived of any such natural reference direction, and the order parameter Ψ''_6 thus becomes dependent on the choice of our reference axis, which is not desirable. On the other hand, calculation of Ψ'_6 does not depend on the direction of the chosen axis, since all possible values of θ' are naturally accounted for within the integral in eq 5. This makes Ψ'_6 particularly well suited to evaluating global order in our systems (which are generally smaller than the typical domain size) in the absence of shear, and is hence preferred over Ψ''_6 for analyzing order in our microscopic simulations. It can be easily shown that, for a perfectly hexagonal lattice, the order parameter $\Psi'_6 = 1$, while for a completely disordered lattice, $\Psi'_6 = 0$. In all these formulations, surfactant molecules i and j are denoted as belonging to a certain micelle A if the distance between any of its two *tail* beads is closer than $d_{ij} = 2$. So, micelles A and B are designated "separate" if the bead center-to-center distance $d_{ij} > 2$ for all tail beads i and j belonging to micelles A and B, respectively.

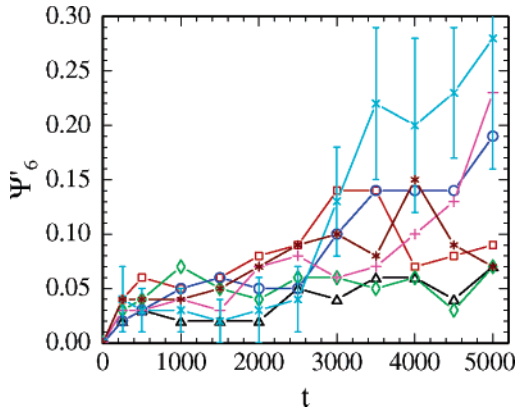

Figure 3. Order parameter Ψ'_6 vs time for different wall velocities $v_w = 0.0(\triangle), 0.1(\square), 0.2(\diamond), 0.5(\bigcirc), 1.0(+), 2.0(\times)$, and $5.0(*)$. Error bars are shown only on one data set for clarity; uncertainties in the other data sets are also of similar magnitude. The lines are guides to the eye.

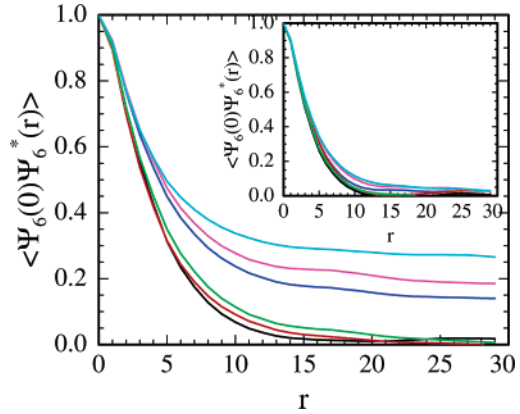

Figure 4. Autocorrelation of the hexatic order parameter vs intermicellar center of mass distance r at different times from bottom to top (t = 500, 1000, 2000, 3000, 4000, and 5000). The main figure corresponds to a sheared system at $v_{wall} = 2.0$, while the inset corresponds to an unsheared system at identical times. The lines are guides to the eye.

Figure 3 shows the order parameter computed for the case of $h = 15$ at different shearing rates. The error bars are fairly large in the figure because of small system sizes, and hence, only qualitative information may be extracted. The order parameter rises only very slowly for the unsheared micelles. As the shear rate is increased, the micelles show a greater tendency to align, as indicated by the increase in the order parameter at any time with the shearing speed. At $v_{wall} = 2.0$, the alignment is particularly significant. However, for much larger speeds (e.g., $v_{wall} = 5.0$), the degree of alignment decreases. The presence of a maximum in this plot is evidently a competition between shear-aided ordering and micelle rupture, which occurs at higher velocities. However, we are unable to explore shear melting[30] of micelles at very high shear rates, as there exists an upper bound on the amount of lateral shear stress that our sliding walls can transmit to the enclosed fluid, as discussed later in more detail.

The difference in alignment of micelles with and without shear may also be analyzed using autocorrelations of a *local* hexatic order parameter as defined in eq 6. This function denoted by $\langle\Psi_6(0)\Psi^*_6(\mathbf{r})\rangle$ is plotted in Figure 4. The correlation would be unity over large distances for perfectly aligned hexagonal layers, whereas it should

(30) Ren, S. R.; Hamley, I. W.; Sevink, G. J. A.; Zvelindovsky, A. V.; Fraaije, J. G. E. M. *Macromol. Theory Simul.* **2002**, *11*, 123.

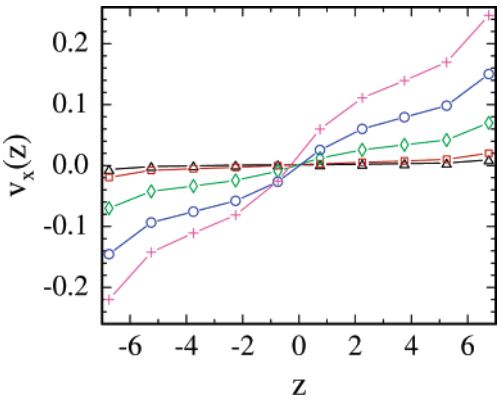

Figure 5. Surfactant velocity profile across the slit cross-section z for different wall velocities $v_{wall} = 0.1(\triangle)$, $0.2(\square)$, $0.5(\diamond)$, $1.0(\bigcirc)$, and $2.0(+)$. Statistical uncertainties in the data are smaller than the size of the symbols. The lines are guides to the eye.

decay instantly to zero for disordered layers. We see that the correlation decays quickly over a short distance (see the inset) for the unsheared micelles but asymptotically approaches a constant value for the sheared micelles. The magnitude of this asymptotic value appreciably increases with time when a finite shear rate is applied; at about halfway through the simulation runs, the correlation lengths span half the size of the simulation box. Beyond this time, the correlation lengths surpass the box dimensions and can no longer be determined. Use of larger system sizes (without such finite-size effects), which require substantially larger computational resources, are needed to determine the scaling of the correlation lengths with time.

One may also compute the variation of the bond angle ($\theta(\mathbf{r}_{ij})$ of eq 5) distributions with time for the sheared and unsheared samples (see Figure S1 of Supporting Information). At the beginning of the simulations, the bond angle distribution for both the sheared and unsheared simulations is *almost* uniform with only a slight peak about the angle at which the lattice prefers to naturally align. With time, the distribution becomes sharply peaked about the shearing direction. However, the unsheared system does not show any significant narrowing of the bond angle distribution. The distribution of the center of mass intermicellar distance (not shown) does not show any differences between the sheared and unsheared micelles. Both distributions start off with a fairly broad peak which becomes narrower over time, as micelles coarsen and adopt more regular arrangements.

It is also instructive to look at the velocity profiles of the block copolymers across the bilayer cross-section z for different wall velocities, as shown in Figure 5. The velocity profiles are not completely linear across the polymer film, but rather show noticeable undulations with inflection points at $z \pm 4$ and $z = 0$. These undulations map out five distinct "bands" across the film thickness. The region around the midplane of the film ($z = 0$), which forms the centermost band, represents the interface between the two micelle layers whose coronas are interacting as the layers slide past each other in opposite directions. This is where the shear rate is highest. A little further away exist the two bands which encompass the micelle cores. The shear rates in these bands are the minimum owing to the tightly bound tail beads within the core of the micelles. This band has the highest effective shear viscosity compared with the rest of the film. Since the shear stress is necessarily constant across planes perpendicular to the z direction (from conservation of momentum in the z direction), the shear rate must be smaller in these regions of high shear viscosity. In the two bands closest to the walls, the shear viscosity is again low and is associated with loosely bound micelle coronas, which naturally results in higher shear rates. These undulations in the shear rate which divide regions according to the shear rates are similar in nature to the shear banding phenomena observed in highly inhomogeneous fluids.[31]

The block copolymer undergoes significant slip at the confining walls, as seen clearly from Figure 5. The velocities of the polymers close to the walls range from 10% to 20% of the imposed wall velocity. This is consistent with the purely repulsive and smooth nature of the walls,[32] in addition to the macromolecular nature of the fluid.[33] The effective shear rate transmitted by the walls to the confined fluid is therefore much lower than that implied by the wall velocities. The overall shear rate across thin films was computed and found to be in the range 0.002−0.035, which translates to extremely high shear rates of 2×10^6 to $3.5 \times 10^7\ s^{-1}$, much higher than the $10\ s^{-1}$ shear rates imposed in experiments. Ultimately, at shearing speeds larger that $v_{wall} = 2.0$, the copolymers were found to lose their "grip" at one of the walls. They were then found to get dragged by one of the surfaces while slipping almost completely at the other. We believe that the relatively smooth walls are ineffective in transmitting shear stresses to the fluid greater than a critical upper-bound shear stress value, which is possibly determined by the competition between the time scales associated with the thermal fluctuation of the block copolymers and that of the sliding motion of the confining walls. The shear stress profile, $\langle\sigma_{xz}\rangle$, across the film thickness was computed using the method of planes[34] (see Figure S2 of Supporting Information). The shear stress increases linearly with wall velocity for $v_{wall} < 1.0$. For $1.0 \le v_{wall} < 2.0$, the slope of the shear stress−wall velocity curve decreases with increasing wall velocity; an indication of shear-thinning behavior. For $v_{wall} = 2.0$, the shear stress decreases, which is consistent with our hypothesis that the wall is unable to transmit stresses larger than 0.052. The normal stress profile σ_{zz} also shows a similar behavior with respect to the shear rate.

It is also important to examine the dependence of the degree of alignment on the film thickness. To this end, we have performed simulations for different wall separations ranging from $h = 10$ to $h = 17$. Figure 6 shows the order parameters obtained for the final configurations, computed as a function of shear rate and film thickness. Clearly, film thickness has a dramatic effect on the alignment of micelles. For very thin films, the micelles are seen to form conjoined micelles across the two layers, resulting in a greater number of defects. This results in less-ordered systems, even after application of shear. In addition, we notice that closely packed micelles are more susceptible to shear disordering. Compare the onset of shear-induced disordering of $v_{wall} = 2.0$ and $v_{wall} = 1.0$ for $h = 15$ and $h = 14$ films, respectively. For very thick films ($h > 15$), the two opposing micelle layers do not sufficiently interact with each other to influence each other's alignment in the direction of shear. Hence, they do not show any significant alignment tendency in response to shear. Consequently, alignment occurs best at an optimum wall separation (film thickness). These results are in excellent agreement with

(31) Spenley, N. A.; Cates, M. E.; McLeish, T. C. B. *Phys. Rev. Lett.* **1993**, *71*, 939.
(32) Arya, G.; Chang, H.-C.; Maginn, E. J. *Phys. Rev. Lett.* **2003**, *91*, 026102.
(33) Priezjev, N. V.; Troian, S. M. *Phys. Rev. Lett.* **2004**, *92*, 018302.
(34) Todd, B. D.; Evans, D. J.; Daivis, P. J. *Phys. Rev. E* **1995** *52*, 1627.

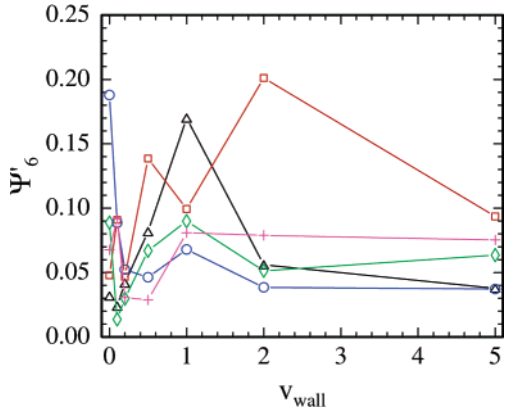

Figure 6. Order parameter Ψ'_6 vs shearing velocity v_{wall} for different film thicknesses: monolayer $h = 10$(+); and bilayer $h = 14$(△), $h = 15$(□), $h = 16$(◇), and $h = 17$(○). The error bars are similar in magnitude to those shown in Figure 3. The lines are guides to the eye.

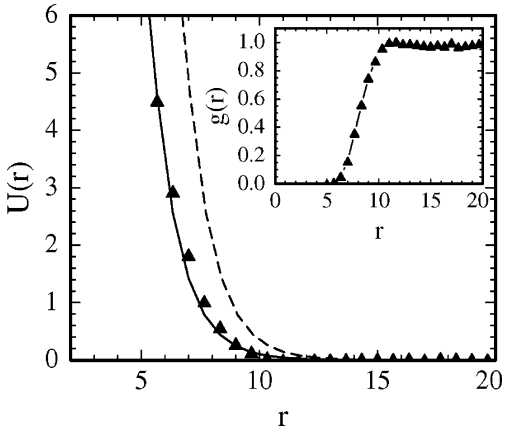

Figure 7. Effective pair potential $U_{eff}(r)$ between micelles, as derived from the pair distribution function $g_{cm}(r)$ (shown in the inset). The solid line represents a fit to the data using a function of the form in eq 2. The dashed line corresponds to the effective potential extrapolated to the bigger micelles formed in our bilayer simulations.

experimental observations. It was also observed that monolayer-thick micellar films ($h = 10$) do not show any tendency to align with shear (see figure), which has also been observed experimentally.

Finally, we would like to point that the shear rates imposed in our computational study are about 6 orders of magnitude larger than those applied in the study of ref 18. This discrepancy should not, however, undermine the conclusions drawn from this study for the following reason: We believe that the correct measure of shear rate that should be compared against experiments is not the *absolute* shear rate but some form of an "effective" shear rate where the shear rate is normalized with the internal relaxation time of the polymers. One such measure of an effective shear rate is the Peclet number (Pe), which is defined as $\mathrm{Pe} = \gamma h^2/D_s$, where γ is the absolute shear rate, h is the thickness of the bilayer, and D_s is the self-diffusivity of the block copolymers in the lateral directions. Since our model block copolymers display dynamics that are several orders of magnitude faster than that of the experimental polymers within the thin film melts of ref 18, the effective shear rates employed in our simulations and the experiments should match quite closely. Indeed, the Peclet numbers computed from our simulations range from 10 to 100, which relates well with the Peclet numbers realized in the experiments of refs 17 and 18.

4. Effective Potential between Micelles

As seen from the above analysis, the molecular-level approach of studying shear-induced ordering of micelles is quite useful for studying the microscopic dynamics of the block copolymer micelles but falls short of accurately describing long-ranged phenomena such as the evolution of global order, unhindered by finite-size effects. This is due to severe computational limitations on system sizes and simulation run times. To this end, we have adopted a multiscale modeling approach where we further coarse-grain the micelles. In this approach, the micelles are modeled as spherical particles which interact with each other through a potential energy function derived from the above molecular-level analysis.

The effective pair interaction potential $U_{eff}(r)$ between micelles' center of masses (separated by distance r) is directly related to the center of mass pair correlation function $g_{cm}(r)$ of an infinitely dilute solution of micelles using the relation

$$U_{eff}(r) = -k_B T \ln[g_{cm}(r)] \qquad (7)$$

At higher concentrations, the micelles experience many-body interactions, and the effective interaction potential becomes more complicated.[35] To obtain $g_{cm}(r)$, we performed several different sets of molecular dynamics simulations for dilute solutions ($\rho = 0.01$) of diblock copolymers at constant temperature for $t = 50\,000$. The block copolymers formed about 5 to 6 stable spherical micelles during the simulations. A typical molecular configuration from one of these simulations is shown in Figure S3 of the Supporting Information. The pair correlation function $g_{cm}(r)$ was obtained by first identifying the micelles' centers of masses and then averaging the instantaneous pair correlation functions at several times during the simulation. Figure 7 shows the pair correlation function and the effective interaction potential using the inversion procedure of eq 7.

There exists one complication in obtaining a coarse-grained potential. The micelles formed at low concentrations of the block copolymers were found to possess mean aggregation numbers of about $\langle n \rangle = 12$ polymer molecules, while the micelles formed at the high polymer concentrations used earlier in this study had mean aggregation numbers of $\langle n \rangle = 29$. Nonetheless, we can make a reasonable extrapolation of the interaction potential to larger micelles from the potential for the smaller micelles. For this purpose, we analyze the interaction potential obtained in Figure 7 more carefully.

The potential in the figure becomes infinite for separations smaller than $r = 5.3$. This distance is equal to twice the radius of gyration of the micelle cores $2r_0$ computed from the simulations. The micelles are hence incapable of penetrating the core of neighboring micelles. The fact that the potential decays slowly to zero within the range $5.3 \le r < 10.5$ shows that the micelle coronas are comparatively softer and can be penetrated by other micelles. The extent of this soft tail correlates well with the diameter of the coronas $D = 9.0$. Clearly, some of the headgroups comprising the corona will extend beyond D, which accounts for a longer tail in the potential. One should note that the *real* block copolymer system which possesses van der Waals interactions between the headgroups should register an attractive portion to this otherwise purely repulsive potential. However, our model of block copolymers (eqs 1−3) precludes attractive interactions between headgroups for the sake of simplicity, and hence, the

(35) Reatto, L.; Levesque, D.; Weis, J. J. *Phys. Rev. A* **1986**, *33*, 3451.

effective potential is also purely repulsive. This soft part of the potential may be fitted with an exponential of the form

$$U_{\text{soft}} = \epsilon' \exp\left[\frac{-(r - \sigma')}{\tilde{r}}\right] \tag{8}$$

where the new energy and length scales of the potential are now ϵ' and σ'. For our simulation data, $\epsilon' = 4.85$ and $\tilde{r} = 1.35$ if we set $\sigma' = 2r_0 = 5.3$. The interaction potential for bigger micelles with which we are concerned with may now be determined. The micelle cores in this case have a diameter of $2r_0 = 6.7$, which correlates well with the notion that the micelle core volume should scale linearly with the aggregation number for the densely packed cores of our well-segregated micelles, i.e., $r_0 \approx \langle n \rangle$. The micelle coronas, on the other hand, were found to be unaffected by the aggregation number. We therefore set $\sigma' = 6.7$, while the value of $\tilde{r}$ remains unchanged. The effective potential corresponding to these new parameters is shown as the dashed line in Figure 7.

Clearly, the above mesoscopic model of micelles increases the accessible length scale to $l' = Dl$ from an initial length scale l in the microscopic simulations. Since $D \approx 10$, we should now be able to access system sizes in the range of micrometers. Similarly, we may obtain an estimate of the time scale by noting that the simulation time $t' \approx (m'l'^2/\epsilon')^{1/2}$. Since the mass of the new elementary particle $m' \approx D^3 m$, $l' \approx Dl$, and $\epsilon' \approx \epsilon$, t' scales as $t' \approx D^{5/2} t$. This implies that our mesoscopic simulations are able to access time scales of several hundred microseconds as compared to about 1 μs for the microscopic simulations.

5. Mesoscopic Shear-Ordering Dynamics

To investigate the ordering mechanism on the scale of typical domain sizes, we perform a second coarse-graining step and replace the self-assembled molecular structures with spherical particles that interact with the effective potential eq 8 for $r > \sigma'$. In addition, we enforce an excluded volume constraint by letting the spheres interact with a steep repulsive potential $U_{\text{excl}} \approx (\sigma'/r)^{12}$ for $r < \sigma'$ with a prefactor chosen so that the forces are continuous at $r = \sigma'$. Note that the units of energy and length in this section are now ϵ' and σ'. This model integrates over the internal degrees of freedom of an individual micelle and, therefore, cannot describe micelle breakup and reformation. The results obtained in this section should, however, be applicable to a wider class of systems, including, for example, colloidal particles.

As in the microscopic simulations, we create a simulation cell that is periodic in the lateral (xy) dimensions and confines the particles in the perpendicular dimension (z) through purely repulsive Lennard-Jones walls. For simplicity, the walls are not represented atomistically here, but are flat and only lead to a confining force in the z direction. The spacing between the walls was set to $h = 2$, in units of $\sigma' + \tilde{r}$, commensurate with a bilayer. Since the walls have no corrugation, they cannot be used to apply the shear as in the first part of this study. Instead, we create a shear stress $\langle \delta\sigma_{xz} \rangle$ by adding a force δf_x to each particle in the x direction that is proportional to its z coordinate, i.e., $\delta f_x = A(z/h)$. We set the z coordinate to zero midway between the walls to ensure that the total force in the x direction is zero and vary the amplitude A. We choose Langevin dynamics to model the motion of micelles and choose a large damping constant to ensure that the dynamics is overdamped (i.e., diffusive Brownian motion). The temperature is set to a low value (0.001), which is far below the melting temperature, so that the system is nearly stationary on relevant simulation time scales in the absence of shear.

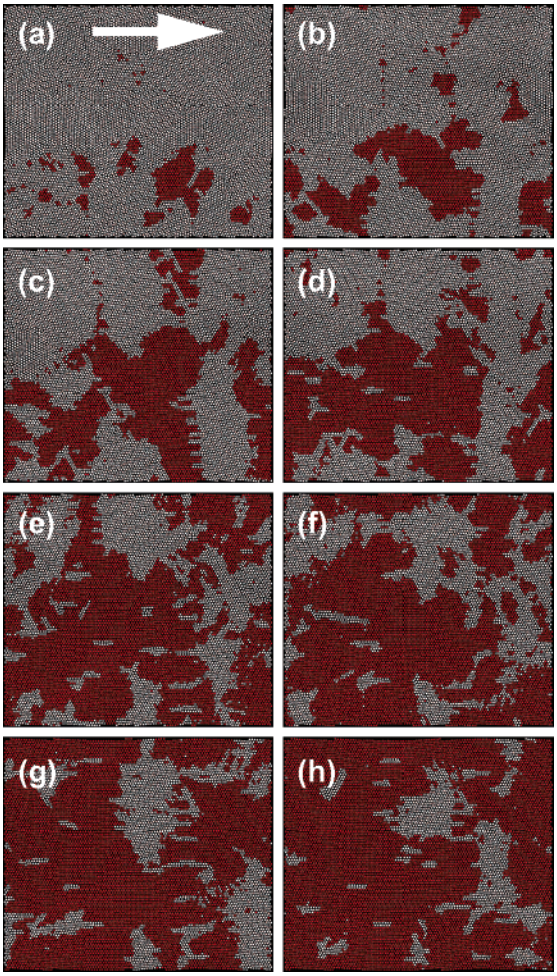

Figure 8. Configurations from a bilayer film simulation containing 20 000 spheres that is sliding under the application of a shear stress $\langle \delta\sigma_{xz} \rangle = 0.28$. Only the top layer, containing 10 000 spheres, is shown at 8 time intervals, separated by $\Delta t = 1\,000$. The shaded particles (red) are those for which $\text{Re}(\Psi_6) > 0.9$, as described in the text.

Initial configurations are created by placing spheres at random into the simulation cell and first running the simulation at an elevated temperature $T = 0.01$. In this way, we anneal local density fluctuations before quenching to the run temperature, $T = 0.001$. At this low temperature, the micelle positions exhibit small thermal fluctuations about their positions. The resulting configuration (see Figure 8a) is free of point defects and is composed of randomly oriented crystalline domains that are well-separated by grain boundaries. This structure strongly resembles the experimental atomic force microscopy (AFM) images[18] of the polymer bilayers.

Figures 8b−h shows several configurations of the system at different times while the layers slide past each other under the influence of a shear stress $\langle \delta\sigma_{xz} \rangle = 0.28$. To monitor the degree of ordering, we calculate the local hexatic order parameter $\Psi_6 = \exp[6i\theta]$, as described above, where θ is the angle that the vectors between neighboring spheres form with the x axis. On the basis of the insight gained in the microscopic simulations, we expect long-range order to develop from those domains with a lattice vector initially oriented with the shear direction. Since for those domains $\text{Re}(\Psi_6) = 1$ and $\text{Im}(\Psi_6) = 0$, we shade those spheres for which $\text{Re}(\Psi_6) > 0.9$ to indicate domains where the hexagonal lattice is oriented in the easy-slip

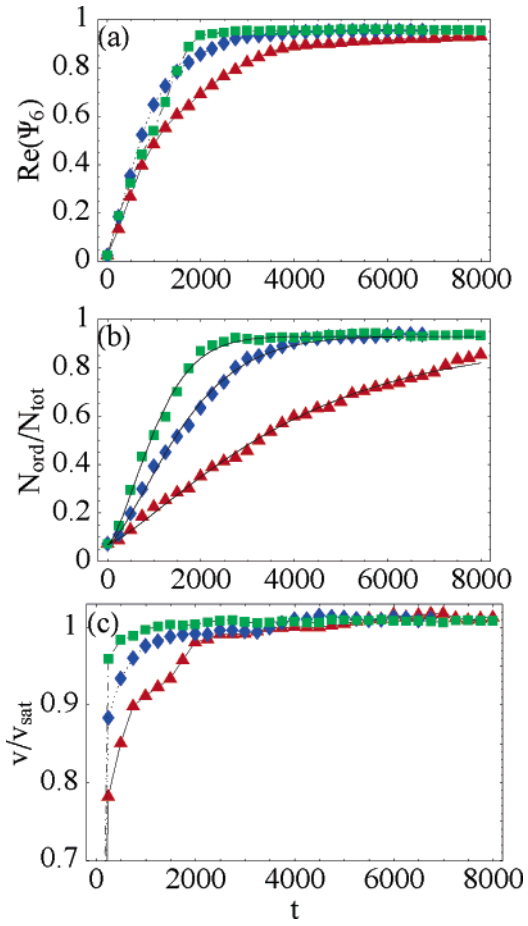

Figure 9. Evolution of order under shearing with shear stresses corresponding to $\langle\delta\sigma_{xz}\rangle = 0.28$(▲), $\langle\delta\sigma_{xz}\rangle = 0.41$(◆), and $\langle\delta\sigma_{xz}\rangle = 0.69$(■). (a) shows the globally averaged value of the hexagonal order parameter $\mathrm{Re}(\Psi_6)$ as a function of time, (b) shows the fraction of spheres $f_{ord}(t) = N_{ord}/N_{tot}$ for which $\mathrm{Re}(\Psi_6) > 0.9$, and (c) shows the average sliding velocity normalized by the saturated velocity of the top layer. The solid lines in (b) show best fits to the Avrami eq 9.

direction. Initially, there are only isolated patches that display this kind of hexagonal order (see Figure 8a). Once the planes begin to shear, these domains grow and quickly merge with other easy-slip oriented domains to form larger consecutive patches (Figure 8b−d). Inspection of Figure 8 and animated sequences show that the growth of the easy-slip domains occurs by motion of the domain walls rather than through the rotation of the lattice in the other domains or through melting and reordering of such domains. At the same time, new oriented domains seem to "nucleate" at the boundaries between misoriented grains. Some of these regions also grow and contribute to the quick increase of global order. In the oriented domains, rows of particles glide past each other in a zigzag-fashion motion about the x direction. In Figure 8d, a cluster of oriented domains already spans the entire plane and continues to quickly absorb the remaining misaligned regions. Our simple mesoscopic model captures the essence of the experimental observation; shear quickly orders an initially random packing of spherical micelles in a bilayer system into a hexagonal lattice in which one of the lattice vectors is parallel to the shear direction.

A more quantitative description of the ordering dynamics can be obtained by computing $\mathrm{Re}(\Psi_6)$ as a function of time. In Figure 9a, we plot the value of $\mathrm{Re}(\Psi_6)$ averaged over the entire film, and in Figure 9b, we plot the fraction of spheres $f_{ord}(t) = N_{ord}(t)/N_{tot}$ for which the local value of

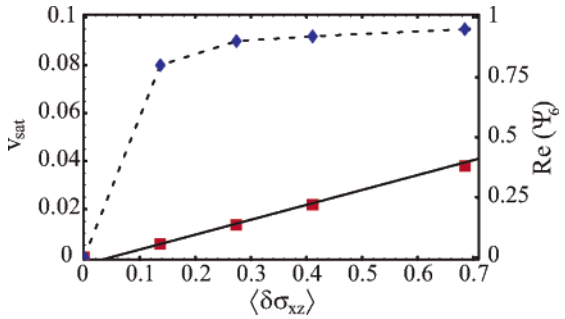

Figure 10. Sliding velocity (■) as a function of applied shear stress. Also shown is the saturation value (◆) of the global value of $\mathrm{Re}(\Psi_6)$.

$\mathrm{Re}(\Psi_6) > 0.9$. While these quantities are not identical, both first seem to rise roughly linearly with time and then gradually saturate at approximately unity. The larger the shear stresses, the more rapidly global order is reached.

The nucleation and growth kinetics of an ordered phase is often described in terms of an Avrami equation[37]

$$\frac{f_{ord}(t)}{f_{ord}(t=\infty)} = 1 - \left(1 - \frac{f_{ord}(t=0)}{f_{ord}(t=\infty)}\right)\exp[-\alpha t^n] \quad (9)$$

In this simple model, individual domains grow at early times with a growth law of $\sim t^n$. However, since oriented domains can only grow by transforming the remaining misoriented regions, the growth saturates exponentially at late times. Best fits to eq 9 (solid lines in Figure 9b) indeed describe the data very well. We obtained exponents n between 1.2 and 1.5. The value of the Avrami exponent n gives some indication as to the operative growth mechanism. In a two-dimensional problem, values of n slightly larger than 1 indicate that the growth of the existing aligned domains is predominantly one-dimensional, while some nucleation of new domains may also be present. Along with alignment, the sliding velocity also increases with time and applied shear stress (Figure 9c). The velocity only saturates once the layers have become fully aligned, and saturation is faster at larger values of $\langle\delta\sigma_{xz}\rangle$. Extending the mesoscopic simulations to very large shear stresses will be unphysical, since we expect the micelles to become unstable and break up, as seen in our microscopic simulations.

Further insight may be gained by measuring the saturated sliding velocity v_{sat} of the layers as a function of applied shear stress. This quantity is shown in Figure 10. For very small shear stresses, v_{sat} is zero, and the system is jammed. This observation is consistent with experiments being conducted in our groups which also see alignment developing only once the applied shear stress exceeds a critical stress. Larger values of the shear stress initiate sliding, and the velocity (and therefore the shear rate) rises linearly with applied shear stress. Also shown in this figure is the saturation value of the order parameter $\mathrm{Re}(\Psi_6)$. This quantity corresponds to the asymptotic value of the curves in Figure 9a and is near 1 as soon as the layers begin to slide.

The length scales in our simulations are now large enough to also obtain spatial correlations in the hexatic order parameter. Figure 11a shows these correlation functions at 10 different times during the simulation with

(36) Harrison, C.; Angelescu, D. E.; Trawick, M.; Cheng, Z. D.; Huse, D. A.; Chaikin, P. M.; Vega, D. A.; Sebastian, J. M.; Register, R. A.; Adamson, D. H. *Europhys. Lett.* **2004**, *67*, 800.
(37) Avrami, M. *J. Chem. Phys.* **1939**, *7*, 1103.

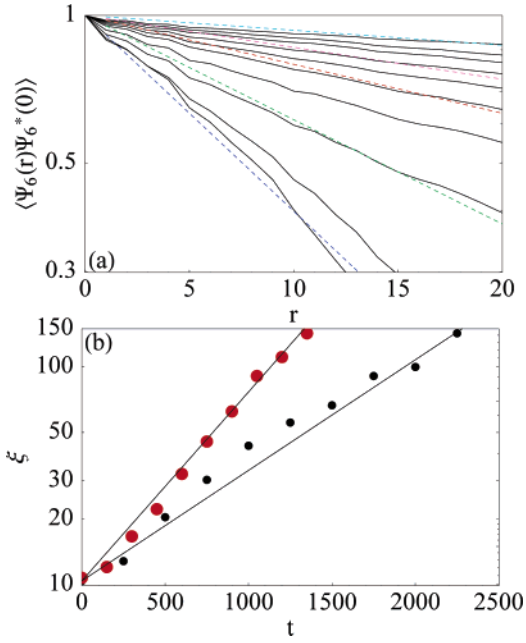

Figure 11. (a) Order parameter correlator as a function of separation r for 10 evenly spaced time intervals. (b) Correlation length ξ obtained from exponential fits to the data in (a) as a function of time t for $\langle\delta\sigma_{xz}\rangle = 0.28$ (small circles) and $\langle\delta\sigma_{xz}\rangle = 0.41$ (large circles) in a semilogarithmic plot. Solid lines represent exponential fits, where the slopes increase proportionally to the sliding velocity (see text).

$\langle\delta\sigma_{xz}\rangle = 0.28$. The correlations are reasonably well described by exponential functions

$$\langle\Psi_6(r)\Psi_6^*(0)\rangle = \exp[-r/\xi] \tag{10}$$

where the fit parameter ξ describes the characteristic length scale of the correlations. The slope of the correlation function decreases with time, in agreement with the development of alignment as already observed in the previous figures, until ξ becomes on the order of the system size. The scaling of the correlation length with time is shown in Figure 11b. Interestingly, for these early times, ξ increases exponentially fast, and the characteristic time scale for domain coarsening increases with increasing sliding velocity. In this regime, our simulations are therefore consistent with a behavior of the form

$$\dot{\xi} \sim \dot{\gamma}\xi \tag{11}$$

where $\dot{\gamma}$ is the effective shear rate.

The origin of this exponential behavior must be related to the mechanism by which alignment occurs. Detailed examination of snapshots such as those shown in Figure 8 demonstrates that, at early times, new aligned regions emerge only from the grain boundaries rather than randomly in the film, while existing already aligned regions rapidly merge. This process forms large clusters of aligned domains that quickly span the entire plane and therefore leads to rapidly growing long-range correlations. The subsequent widening of the aligned regions then proceeds algebraically rather than exponentially (see Figure 9), because the grain boundaries cannot move more rapidly than the particles themselves. The exponential coarsening at early times, however, is remarkable, because in the absence of a shear stress, experiments show a much slower coarsening rate; i.e., power-law coarsening with exponents generally less than $^1/_2$.[36] This provides a basic explanation for the efficiency of the ordering process in the presence of shear.

Finally, we would like to point out that our system of highly segregated micelles being sheared laterally is quite analogous to the problem of sheared colloidal suspensions. Certainly, the alignment of three-dimensional colloidal suspensions via shearing is not entirely a new concept.[38−40] However, the influence of shear on *bilayers* of colloids has not been examined so far; the only study coming closest to this concerns shearing of a four-colloidal-particles-thick suspension.[41] We believe that several insights on the ordering of sheared and unsheared spherical micelles may be borrowed from the colloids literature, especially those pertaining to the coarsening kinetics and scaling behavior of colloids.[42]

6. Conclusions

We have studied shear-induced ordering in bilayers of self-assembled block copolymer spheres using two computational approaches on different length and time scales. In the first approach, the block copolymers have been explicitly represented using bead and spring models with suitable interaction parameters which mimic microphase separation. Using this approach, we have successfully demonstrated the microscopic mechanism responsible for shear-induced alignment of block copolymer spheres. The hexagonally arranged micelles in the two layers flow in their respective shearing directions. This causes the micelles to adjust their positions such that the frictional drag between the oppositely flowing layers is minimized, which leads to the alignment of one of their hexagonal lattice vectors in the direction of applied shear. More importantly, we show that the micelles do not need to break up and re-form to align. We also demonstrate the sensitivity of the alignment on the film thickness, in agreement with experiments.

These simulations are, however, unable to give any reliable information on the growth of locally ordered domains into global long-range order because of system size limitations. To this end, we have extended the length and time scales by first extracting an effective interaction potential between microscopic micelles and then replacing the aggregates with spheres that interact with this potential. As in experiments, an initially randomized morphology of locally ordered hexagonal domains develops into a macroscopically ordered hexagonal lattice. This process occurs by the motion of the domain walls (grain boundaries) rather than by grain rotation or melting. In agreement with experiments, we find that ordering occurs only above a certain threshold stress. Although the results presented here were obtained at a very low temperature, tests at higher temperatures showed no strong effect of temperature on the efficiency of the ordering process within the present model.

An analysis of the autocorrelation of the hexatic order parameter reveals that order initially increases exponentially rapidly in the presence of shear, which underscores the efficiency of external fields in creating ordered structures. The origin of this exponential behavior is not fully understood at present. Its relation to the details of the ordering mechanism at the grain boundaries will

(38) Ackerson, B. J.; Pusey, P. N. *Phys. Rev. Lett.* **1988**, *61*, 1033.
(39) Chen, L. B.; Zukoski, C. F.; Ackerson, B. J.; Hanley, H. J. M.; Straty, G. C.; Barker, J.; Glinka, C. J. *Phys. Rev. Lett.* **1992**, *69*, 688.
(40) Stevens, M. J.; Robbins, M. O.; Belak, J. F. *Phys. Rev. Lett.* **1991**, *66*, 3004.
(41) Cohen, I.; Mason, T. G.; Weitz, D. A. *Phys. Rev. Lett.* **2004**, *93*, 046001.
(42) Boyer, D.; Viñals, J. *Phys. Rev. Lett.* **2002**, *89*, 055501.

therefore be examined in future work. The fact that our simple mesoscopic model reproduces many aspects of the experiments is a strong indication that it already contains the most essential physical input required to understand shear ordering. The present results also demonstrate that insight into complex nonequilibrium processes can be gained through the use of a sequentially coarse-grained description that retains key elements at each level.

Acknowledgment. This work was supported by the NSF (MRSEC Program) through the Princeton Center for Complex Materials (DMR 0213706). Additional support was provided by ACS-PRF (grant 38165-AC9) and DOE (grant DE-FG02-01ER15121). We gratefully acknowledge stimulating discussions with Prof. Richard Register.

Supporting Information Available: Evolution of nearest-neighbor micelles center-to-center bond angle distribution with time, variation of the shear stress and normal stress with respect to the wall sliding velocity, micelle configuration at low surfactant concentration used for obtaining the potential of mean force, and close-up view of micelle packing in Figure 8b. This material is available free of charge via the Internet at http://pubs.acs.org.

LA0516476